Title:

Simulation on Flow and Soot Deposition in Diesel Particulate Filter

Authors:
Kazuhiro YAMAMOTO and Shinya OHORI

Affiliation:
Department of Mechanical Science and Engineering, Nagoya University
Furo-cho, Chikusa-ku, Nagoya-shi, Aichi 464-8603, Japan

Type of article:
Paper

Address of the corresponding author
Address: Furo-cho, Chikusa-ku, Nagoya-shi, Aichi 464-8603, Japan
Telephone number: +81-52-789-4471
Fax number: +81-52-789-4471
E-mail address: kazuhiro@mech.nagoya-u.ac.jp

Title:
Simulation on Flow and Soot Deposition in Diesel Particulate Filter

Authors:
Kazuhiro YAMAMOTO and Shinya OHORI

Abstract:
To reduce particulate matters (PM) including soot in diesel exhaust gas, a diesel particulate filter (DPF) has been developed. In the after-treatment of exhaust gas, it traps PM when exhaust gas passes its porous wall. An increase of PM accumulation could cause technological problems due to the higher filter back-pressure. This can result in a subsequent worsening of fuel efficiency and a decrease in engine output. However, it is difficult to observe the phenomena in DPF experimentally. In this study, we simulated the flow with soot deposition by the lattice Boltzmann method (LBM). Here, to discuss the flow in the real cordierite filter, a tomography-assisted simulation was conducted. The inner structure of the filter was scanned by a 3D X-ray CT technique. The local velocity and pressure distributions in the filter were clearly visualized. To model the soot deposition, a parameter of soot deposition probability (PD) was used. Results show that the pressure drop increases as more soot is deposited. When the soot deposition probability of PD is larger, the soot deposition region is limited to the filter wall surface, corresponding to the surface filtration. The pressure drop is smaller as PD is increased.

Key words: diesel engine, after-treatment, particle filtration, soot, diesel particulate filter, lattice Boltzmann method, X-ray CT

1. INTRODUCTION

Diesel vehicles such as buses and trucks have high thermal efficiency, and represent an effective means of reducing CO_2 emissions when compared with equivalent gasoline vehicles. Therefore, the use of diesel vehicles should be encouraged. However, the exhaust gas of diesel vehicles contains particulate matters (PM) and NOx that cause environmental pollution [**1**-**3**]. In particular, the exhaust PM in the form of nanoparticles of diameters less than 100 nm is reported to be harmful to human health. For this reason, a number of after-treatment technologies have been developed as countermeasures against diesel exhaust PM. One of these is a diesel particulate filter (DPF) that has been recently incorporated into diesel vehicles to absorb and remove PM [**4-8**].

Figure 1 shows a cordierite filter used in this study. In simple explanation of DPF, it traps PM when the exhaust gas passes its porous wall (**Fig. 1(b)**). The filtration efficiency can be as high as 99 % [**8**]. However, an increase of PM accumulation could cause technological problems due to the higher filter back-pressure. This can result in a subsequent worsening of fuel efficiency and a decrease in engine output. To remove PM by catalytic oxidation, a new technique with a heat recovery function has been proposed [**9**].

It is known that the pressure loss in DPF is the sum of three pressure losses: one at the channel inlet and outlet, another along the channel, and third within the porous sidewall with soot deposition [**10**]. The pressure loss is the largest within the porous wall, making it important to clarify fluid flow and deposition of fine nanoparticles such as soot on the filter substrate, which has an area of about a few hundred μm^2. So far, the process of PM deposition and subsequent pressure changes have been modeled [**4**]. However, measuring the flow and pressure within the porous sidewall with microscopic structure is difficult. Therefore, using a numerical analysis, we have visualized the phenomena inside DPF as well as the flow field, which could be an effective approach to reduce the pressure losses caused by soot deposition [**11-17**].

In the present study, the relationship between the amount of soot deposition and the pressure loss is clarified by the simulation. The flow and the soot deposition inside DPF are described by a lattice Boltzmann method (LBM), which is an effective method for analysis of the flow inside the porous material. The porous structure of an actual DPF is first analyzed using an X-ray computed tomography (CT) [**15-17**]. The X-ray CT is non-destructive system, and it has a potential for the inspection of thermal damage, soot and ash depositions in DPF [**18**].

2. ANALYTICAL MODEL

2.1 Lattice Boltzmann method

This section briefly explains the principles of LBM [**19-22**], where the flow is analyzed based on the processes of translation and collision of particles. Recently, LBM has been widely used to simulate the exhaust gas flow in DPF [**23-25**]. By using CT data of inner structure of DPF, we have simulated the deposition and oxidation of soot [**15-17**]. The distribution function of the particles is used to describe the translation process, whereby the distribution function moves by one lattice at each time setup, and the collision process, whereby the distribution function is relaxed to the equilibrium distribution due to collision. In this study, a three-dimensional calculation was performed using a d3q15 model with space discretization on cubic lattices [**26**].

Next, the numerical approach is explained. Detailed procedures of the deposition and oxidation of soot particles are available in other papers [**11-17**]. In general, it is known that the pressure loss in DPF increases along with the soot deposition [**4-8**]. To simulate this phenomenon, the effect of deposited soot layer on the flow field of exhaust gas must be taken into consideration. However, in our previous studies [**11-17**], we did not consider the flow through the deposited soot layer. To predict the pressure loss more precisely, this effect should be included in the numerical model. Here, by assuming that the friction force acts on exhaust gas in the soot layer and by introducing an external force term in the lattice Boltzmann equation, the effect of deposited soot layer is considered [**24**]. In an incompressible model, the flow is calculated based on the distribution function of pressure. The lattice Boltzmann equation that includes the external force term and the local equilibrium distribution function are expressed by the following formulas (1) and (2), respectively:

$$f_{p,i}(\boldsymbol{x}+\boldsymbol{e}_i\delta_t,t+\delta_t)-f_{p,i}(\boldsymbol{x},t)=-\frac{1}{\tau_p}[f_{p,i}(\boldsymbol{x},t)-f_{p,i}^{eq}(\boldsymbol{x},t)]-\frac{\tau_p-0.5}{\tau_p}F_i \qquad (1)$$

$$f_{p,i}^{(eq)}=w_i\left\{p+p_0\left[3\left(\frac{\boldsymbol{e}_i\cdot\boldsymbol{u}}{c^2}\right)+\frac{9}{2}\left(\frac{\boldsymbol{e}_i\cdot\boldsymbol{u}}{c^2}\right)^2-\frac{3}{2}\left(\frac{\boldsymbol{u}}{c}\right)^2\right]\right\} \qquad (2)$$

where w_i = 1/9 (i = 1−6), 1/72 (i = 7−14), and 2/9 (i = 15), $c = \delta_x/\delta_t$, δ_x and δ_t represent the lattice space and time step, respectively, and p_0 represents atmospheric pressure. The relaxation time τ_p in Eq. (1) is the value corresponding to the coefficient of kinematic

viscosity, ν, given by

$$\nu = \frac{2\tau_p - 1}{6}\frac{\delta_x^2}{\delta_t} \qquad (3)$$

The pressure p, the velocity $\boldsymbol{u}$, the external force $\boldsymbol{f}$, and the external force term F_i can be obtained from the following formulas:

$$p = \sum_i f_{p,i} \qquad (4)$$

$$\boldsymbol{u} = \sum_i \boldsymbol{e}_i f_{p,i} / p_0 + 0.5\boldsymbol{f}\delta_t \qquad (5)$$

$$\boldsymbol{f} = -\frac{\nu}{\kappa}\boldsymbol{u} \qquad (6)$$

$$F_i = \frac{-3\boldsymbol{f}\cdot(\boldsymbol{e}_i - \boldsymbol{u})}{c^2} f_{p,i}^{(eq)} \qquad (7)$$

where κ represents the permeability. It is known that the permeability of the soot layer depends on the flow of the exhaust gas that passes through the sidewall, the diameter of the primary soot particles, and the Pe number, which is defined by the diffusion coefficient of an aggregate of soot particles. At the exhaust gas temperature of 573 K, the typical permeability of the soot layer has been reported to be 2.0×10^{-14} m^2 [**27**]. As explained in section 2.2, we did not consider the soot particle size. Then, the constant value of $\kappa = 2.0 \times 10^{-14}$ m^2 was used in the present study.

On the other hand, the soot concentration in the gas phase is obtained based on the distribution function of the soot concentration. The soot deposition model is explained in the next section. The equations for the evolution and equilibrium distribution function are expressed by the following formulas (8) and (9), respectively:

$$f_{c,i}(\mathbf{x} + \mathbf{e}_i\delta_t, t + \delta_t) - f_{c,i}(\mathbf{x}, t) = -\frac{1}{\tau_c}[f_{c,i}(\mathbf{x}, t) - f_{c,i}^{(eq)}(\mathbf{x}, t)] \qquad (8)$$

$$f_{c,i}^{(eq)} = w_i Y_c \left\{1 + 3\left(\frac{\mathbf{e}_i\cdot\mathbf{u}}{c^2}\right) + \frac{9}{2}\left(\frac{\mathbf{e}_i\cdot\mathbf{u}}{c^2}\right)^2 - \frac{3}{2}\left(\frac{\mathbf{u}}{c}\right)^2\right\} \qquad (9)$$

Similar to the pressure, the soot concentration (soot mass fraction) is obtained by

$$Y_c = \sum_i f_{c,i} \qquad (10)$$

As for the relaxation time τ_c, the same value of τ_p in Eq. (3) was used to determine the soot concentration field.

2.2 Soot deposition model

The adsorption of soot particles is affected by the Brownian diffusion, impaction and interception effects, gravity, and physical properties of the filter surface [**28**]. Additionally, the real diesel soot particle of PM is not spherical and is an aggregate composed by several primary particles. When the actual size of PM is taken into consideration, the analysis must be performed at a nanometer scale, which means that a numerical cost will be consequently huge. Then, we only monitored the soot mass fraction in both the gas phase and the deposited soot region. In order to simulate the soot deposition on the filter substrate, the soot deposition probability of P_D was adopted, and the above effects were implicitly considered [**15,17**]. However, the value of the soot deposition probability could depend on the filter substrate conditions or the soot particle properties. Then, the parametric study was conducted by changing P_D widely.

The method of soot deposition is explained in **Fig. 2**. It shows an area around the filter substrate on which the soot is deposited at a given time (time step IT_1). The soot is transported to the lattice point by the flow. In this region, soot at a ratio of P_D is deposited, while that at $(1-P_D)$ is not deposited and is rebounded into the flow and transported again. In this model, an exfoliation of the soot layer due to the flow is not taken into consideration. As the calculation proceeds, the sum of the soot concentration at the lattice point is increased. At some time, due to the soot deposition, the mass fraction of soot reaches unity at time step IT_2. Then, the point near the filter substrate (or soot layer) where the soot concentration reaches unity is set as the solid phase, instead of the gas phase. From the next time step ($IT_2 + 1$), the deposition region, where the sum of soot concentration is counted, is moved to one point ahead of the original boundary. In this way, the soot deposition layer grows.

2.3 Calculation domain and boundary conditions

The internal structure of the filter wall was obtained using a three-dimensional X-ray CT measurement for the fluid simulation inside the actual filter. **Figure 3** shows a CT image of the filter [**16**]. Three slice images of the filter at *xy*, *yz*, *xz* planes are shown. The spatial resolution was 1 μm/pixel. The image area is 400 μm (x) × 400 μm (y) × 200 μm (z). The exhaust gas passes through the filter wall in the x-direction. Then, x is the

distance normal to main flow direction. Based on CT data, the averaged porosity of the filter was about 0.4, and the typical pore size of the filter substrate was about 10 μm. Intricate porous structure with variety of pore size is well observed. In the simulation, a part of inner structure was used, whose porosity and pore size were the same as those of the whole area of CT data.

Figure 4 shows the calculation domain with the coordinate system used in this study. The filter sidewall was set at the centre of the calculation domain, with the entrance zones set before and after the filter. In the coordinate system, the direction of the exhaust gas flow passing through the filter and the directions perpendicular to the flow direction were expressed using x, y, and z, and the velocity components corresponding to these directions were expressed using u, v, and w, respectively. The sizes of calculation domain were 400 μm in x direction and 80 μm in y and z directions. Since the spatial resolution of the X-ray CT measurement was 1 μm/pixel, the grid size of the simulation was 1 μm. The surface roughness of the porous filter substrate was well visualized, but it was much larger than the size of the soot aggregates. The number of calculation lattices was 401 (x) × 81 (y) × 81 (z).

Next, the boundary conditions are explained. At the inlet, the exhaust gas containing soot with mass fraction of 1.6×10^{-4} [**17**] was flowed into the filter at a velocity of U_{in}. The exhaust gas temperature was 573 K (300ºC). The slip boundary was applied as a symmetrical boundary at the four sidewalls (top, bottom, right, and left). The outlet was set as a free outflow boundary with a constant pressure (atmospheric pressure).

3. RESULTS AND DISCUSSION

3.1 Flow field

First of all, before simulating the soot deposition process, the flow inside the filter was visualized. The cold flow at room temperature was used. **Figure 5** shows the velocity field inside the filter, which is under steady state with small velocity perturbation. The inflow velocity of U_{in} was 1.0 m/s. The velocity vector is shown, with filter substrate by gray region. Three different slice images are shown at (a) x = 50 μm, (b) x = 200 μm, and (c) x = 350 μm. It is seen that the ceramic filter has many small pores. Then, the velocity and its direction are largely changed when the flow passes through the porous wall.

Next, we examined the pressure field inside the filter. The result is shown in **Fig. 6**. This pressure is the averaged value in the yz plane. For comparison, the porosity, ε, is shown in this figure. The filter wall is roughly located in the range of 50 μm < x < 350

μm, and the porosity outside the filter is unity. These results were obtained when the inflow velocity across the filter wall was set to be 1 m/s. The soot deposition was not considered in this case. It looks like the pressure drop from 1.6 to 1.0 may be too large. As the inflow velocity is lower, the pressure drop is smaller. It is well known that, in the case of homogenous porous media, the pressure linearly decreases along the flow direction, and the pressure gradient is constant [**29**]. However, as seen in this figure, since the porosity inside the filter wall is largely varied from 0.2 to 0.9, the pressure gradient is changed. Therefore, depending on the non-uniformity of pore-structure, both flow and pressure are largely changed inside the filter.

Here, to confirm the validity of the numerical scheme, simulation results were compared with the empirical equation. The idea is based on the porous media flow theory [**29**]. The hydraulic radius, R_h, and the equivalent diameter of the filter substrate, D_p are as follows:

$$R_h = \frac{volume\ \ available\ \ for\ \ flow}{total\ \ wetted\ \ surface} \qquad (11)$$

$$D_p = 6R_h \frac{1-\varepsilon}{\varepsilon} \qquad (12)$$

The friction factor and the Reynolds number of Re are defined by

$$\text{Friction factor} = \left(-\frac{dp}{dx}\right)\frac{D_p}{\rho_0 U_{in}^2}\frac{\varepsilon^3}{(1-\varepsilon)} \qquad (13)$$

$$\text{Re} = \frac{U_{in} D_p}{\nu(1-\varepsilon)} \qquad (14)$$

The empirical equation, which is called an Ergun equation, is

$$\text{Friction factor} = 150/\text{Re} + 1.75 \qquad (15)$$

Figure 7 shows simulation results, compared with the Ergun equation. The inflow velocity was in the range of 0.2 to 20 m/s. Needless to say, the filter substrate is a porous material. In the simulation, a part of CT data was selected. If its size is too small,

there may be only one or two route of the flow across the filter. Then, it is not appropriate to discuss the flow field inside DPF. However, as seen in this figure, for all cases, a good agreement with the Ergun equation is observed. Thus, although the computational domain was limited in our tomography-assisted simulation, it is confirmed that we could discuss the effect of soot deposition on the flow and pressure in the real filter.

3.2 Soot deposition

Finally, the soot deposition was simulated. **Figure 8** shows the temporal changes in the amount of soot deposition at P_D = 0.1, 0.5, and 1.0, respectively. The soot density of ρ_s shown on the vertical axis was determined by the deposited soot mass per total filter volume, which is given by

$$\rho_s = \frac{\rho_c \cdot V_s}{\alpha \cdot V_F} \qquad (16)$$

Here, ρ_c represents the density of the deposited soot layer, which is 380 kg/m^3 of carbon black. V_s represents the volume of the soot layer formed in the calculation domain, and V_F represents the sidewall volume, and α represents the ratio of the filter volume (the sum of the sidewall volume and the flow volume) to the sidewall volume. In the simulation, the high loaded condition was considered. Then, the soot mass loading of 3 ~ 4 g/l occurs within 120 seconds. This situation was observed in the experiments using an engine test bench [**8**]. As shown in this figure, the amount of soot deposition at the same elapsed time is decreased with a decrease of P_D.

Next, the soot deposition area was examined. **Figure 9** shows the *xy* cross-sectional distributions of soot deposition region at z = 32 μm at time of t = 88 s. The soot deposition probability of P_D is 0.1, 0.5, and 1.0. It should be noted that the soot deposition occurs in the range of x < 150 μm. That is, most of the deposition is observed in the upstream part of DPF, corresponding to our previous simulation results and experiments [**15**]. Then, to discuss the soot deposition area, the enlarged figures around the filter wall surface are shown. For all cases, the soot density is 2.8 g/l. Expectedly, as the soot deposition probability is larger, more soot is deposited on the filter wall surface, corresponding to the surface filtration.

Wirojsakunchai et al., have reported the experimental data to explain DPF filling process with the PM trap by the conceptual model [**4**]. When the PM starts to deposit in the clean DPF, the PM is initially collected on the inside walls of the large substrate

pore (stage 1), which is called a depth filtration. During this stage, the pressure drop is not largely changed. When more PM accumulates, the pressure increases very largely due to the pore bridging (stage 2). After that, a thin "soot cake layer" of PM begins to develop at the filter inlet, which is called a surface filtration. In this case, a linear and smaller pressure rise is observed as the cake layer grows (stage 3). In this simulation, the above-mentioned phenomena were observed.

Next, the relationship between the amount of soot deposition and the pressure drop across the filter was examined by changing the soot deposition probability. Results are shown in **Fig. 10**. At $P_D = 0.1$, at the initial stage, the pressure slightly changes, and then rises abruptly. At later stages, the pressure drop is increased almost linearly. Thus, a similar tendency to the experimental data is observed [**4**]. Interestingly, for the equivalent amount of soot deposition, the pressure drop is larger as P_D is smaller. As shown in **Fig. 9**, at $P_D = 1.0$, more soot is deposited on the filter wall surface, corresponding to the surface filtration. It has been reported that the pressure drop caused by the surface filtration is relatively smaller, because the soot cake layer has porous structure with large porosity [**27**]. On the other hand, at $P_D = 0.1$, the soot is deposited inside the filter sidewall, corresponding to the depth filtration. In this case, the flow is forced to pass through the narrower substrate pore due to the soot deposition. Resultantly, even at the same soot density, the pressure drop is larger.

4. CONCLUSIONS

In this study, we simulated the flow with soot deposition by the LBM. Here, to discuss the flow in the real cordierite filter, the tomography-assisted simulation was conducted. The inner structure of the filter was scanned by the 3D X-ray CT technique. The flow through the deposited soot layer was considered to predict the pressure loss precisely. To model the soot deposition, the parameter of soot deposition probability was adopted. By changing P_D widely, the parametric study was conducted to monitor the soot deposition area and the amount of soot deposition. The following results were obtained.

(1) The inner structure of DPF was well visualized. The typical pore size of the filter substrate is about 10 μm, and the intricate structure with small pores exists inside the filter wall. Even in cold flow, the complex flow pattern was observed due to the non-uniformity of pore structure. Based on the flow characteristics in the range of 0.2 to 20 m/s, the simulation results show a good agreement with the empirical equation of the porous media flow.

(2) During DPF filling with soot, there are three stages: (i) soot deposition on the inside

walls of large substrate pore, (ii) pore bridging deposition, (iii) soot layer formation at the filter inlet. According to these deposition processes, the pressure slightly changes, then rises abruptly, and linearly increases in the pressure curve vs. the amount of deposited soot. These deposition processes were in accordance with the reported experimental data.

(3) The pressure drop increases as the soot deposition is progressed. As the soot deposition probability is larger, more soot is deposited due to the surface filtration, resulting in the smaller pressure drop.

ACKNOWLEDGEMENTS

This work was partially supported by the Rare Metal Substitute Materials Development Project, New Energy and Industry Technology Development Organization (NEDO) in Japan.

REFERENCES

(1) **Stein, H. J.** Diesel Oxidation Catalysts for Commercial Vehicle Engines: Strategies on Their Application for Controlling Particulate Emissions. Appl. Catal. B-Environ., 1996, **10**, 69-82.

(2) **Clerc, J. C.** Catalytic Diesel Exhaust After-treatment, Appl. Catal. B-Environ., 1996, **10**, 99-115.

(3) **Stratakis, G. A., Psarianos, D. L., and Stamatelos, A. M.** Experimental Investigation of the Pressure Drop in Porous Ceramic Diesel Particulate Filters. Proc. Inst. Mech. Eng. Part D-J, Automob. Eng., 2002, **216**, 773-784.

(4) **Wirojsakunchai, E., Schroeder, E., Kolodziej, C., Foster, D. E., Schmidt, N., Root, T., Kawai, T., Suga, T., Nevius, T., and Kusaka, T.** Detailed Diesel Exhaust Particulate Characterization and Real-Time DPF Filtration Efficiency Measurements During PM Filling Process, SAE paper 2007-01-0320, 2007.

(5) **Yamada, H. and Goto, Y.** Optimization of PM Measurements with a Number Counting Method. SAE Paper 2008-01-2436, 2008.

(6) **Johnson, T. V.** Diesel Emissions in Review. SAE Paper 2011-01-0304, 2011.

(7) **Rakovec, N., Viswanathan, S., Foster, D.** Micro-scale Study of DPF Permeability as a Function of PM Loading. SAE Paper 2011-01-0815, 2011.

(8) **Tsuneyoshi, K., Takagi, O., Yamamoto, K.** Effects of Washcoat on Initial PM Filtration Efficiency and Pressure Drop in SiC DPF. SAE Paper 2011-01-0817, 2011.

(9) **Obuchi, A., Uchisawa, J., Ohi, A., Nanba, T., Nakayama, N.** A Catalytic Diesel Particulate Filter with a Heat Recovery Function. Topics in Catalysis, 2007, **42**, 267-271.

(10) **Konstandopoulos, A. G.** Flow Resistance Descriptors for Diesel Particulate Filters: Definitions, Measurements and Testing, SAE Paper 2003-01-0846, 2003.

(11) **Yamamoto, K., Takada, N. and Misawa, M.**, Combustion Simulation with Lattice Boltzmann Method in a Three-dimensional Porous Structure, Proc. Comb. Inst., 2005, **30**, 1509-1515.

(12) **Yamamoto, K. and Ochi, F.**, Soot Accumulation and Combustion in Porous Media, *J. Energy Inst*., 2006, **79**, 195-199.

(13) **Yamamoto, K., Satake, S., Yamashita, H., Takada, N. and Misawa, M.**, Lattice Boltzmann Simulation on Porous Structure and Soot Accumulation, Mathematics and Computers in Simulation, 2006, **72**, 257-263.

(14) **Yamamoto, K. and Takada, N.**, LB Simulation on Soot Combustion in Porous Media, Physica A, 2006, **362**, 111-117.

(15) **Yamamoto, K., Satake, S., Yamashita, H., Takada, N., and Misawa, M.**, Fluid Simulation and X-ray CT Images for Soot Deposition in a Diesel Filter, the European Physical Journal, 2009, **171**, 205-212.

(16) **Yamamoto, K., Nakamura, M., Yane, H., and Yamashita, H.**, Simulation on Catalytic Reaction in Diesel Particulate Filter, Catalysis Today, 2010, **153**, 118-124.

(17) **Yamamoto, K., Yamauchi, K., Takada, N., Misawa, M., Furutani, H., Shinozaki, O.**, Lattice Boltzmann Simulation on Continuously Regenerating Diesel Filter, Philosophical Transactions A (The Royal Society, London), 2011, **369**, 2584-2591.

(18) **Zandhuis, J. A., Finney, C. E. A., Toops, T. J., Partridge, W. P., Daw, C. S., Fox, T.** Nondestructive X-ray Inspection of Thermal Damage, Soot and Ash Distributions in Diesel Particulate Filters. SAE Paper 2009-01-0289, 2009.

(19) **Hou, S., Shan, X., Zou, Q., Doolen, G. D. and Soll W. E.** Evaluation of Two Lattice Boltzmann Models for Multiphase Flows, J. Computational Physics, 1997, **138**, 695-713.

(20) **Filippova, O. and Hanel, D.** Lattice-Boltzmann simulation of Gas-particle Flow in Filters, J. Comput. Physics B, 2003, **26**, 197-200.

(21) **Inamuro, T., Yoshino, M. and Ogino, F.** Lattice Boltzmann Simulation of Flows in a Three-dimensional Porous Structure, Int. J. Num. Methods in Fluids, 1999, **29**, 737-748.

(22) **Chen S. and Doolen, G. D.** Lattice Boltzmann Method for Fluid Flows, Annu. Rev. Fluid Mech., 1998, **30**, 329-364.

(23) **Muntean, G. G., Reactor, D., Herling, D., Lessor, D., Khaleel, M.** Lattice-Boltzmann Diesel Particulate Filter Sub-Grid modelling – A Progress Report. SAE Paper 2003-01-0835, 2003.

(24) **Hayashi, H.** Lattice Boltzmann Method and its Application to Flow Analysis in Porous Media, R&D Review of Toyota CRDL, 2003, **38**, 17-25.

(25) **Dillon, H., Stewart, M., Maupin, G., Gallant, T., Li, C., Mao, F., Pyzik, A., Ramanathan, R.** Optimizing the Advanced Ceramic Material for Diesel Particulate Filter Applications. SAE Paper 2007-01-1124, 2007.

(26) **Qian, Y. H., D'Humie'res. D. and Lallemand, P.** Lattice BGK Models for Navier-Stokes Equation, Europys. Lett., 1992, **17**, 479-484.

(27) **Konstandopoulos, A. G., Skaperdas, E.**, Microstructural Properties of Soot Deposits in Diesel Particulate Traps, SAE paper 2002-01-1015, 2002.

(28) **Hinds, W. C.**, Aerosol Technology Second Edition, 1999 (John Wiley & Sons).

(29) **Bird, R. B., Strwart, W. E., and Lightfoot, E. N.**, Transport phenomena, 1960 (John Wiley & Sons).

APPENDIX

Notation

c = advection speed in LB coordinate

D_p = equivalent diameter

$\boldsymbol{e}$ = unit vector for advection speed in LB coordinate

$\boldsymbol{f}$ = external force

F_i = external force term

$f_{p,\alpha}$ = distribution function of pressure

$f_{s,\alpha}$ = distribution function of soot in gas phase

IT = time step

p = pressure

P_D = soot deposition probability

Re = Reynolds number

R_h = hydraulic radius

t = time

$\boldsymbol{u}$ = velocity vector of (u, v, w)

U_{in} = inlet velocity

x = direction normal to the filter

y = direction perpendicular to x

z = direction perpendicular to x

Y_c = mass fraction of soot

ε = porosity

κ = permeability

ν = kinematic viscosity

ρ = density

τ = relaxation time

Subscripts

0 = reference condition

C = properties of soot in gas phase

F = properties of filter

in = value at inlet

out = value at outlet

s = properties of soot per total filter volume

α = number of advection speed in LB coordinate

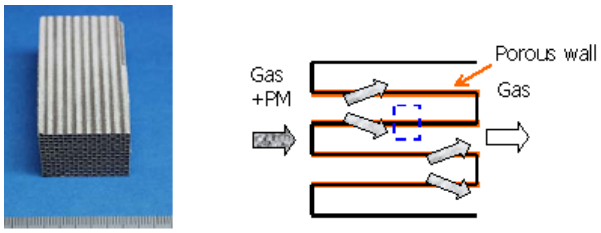

Fig. 1 (a) Photograph of cordierite filter, and (b) PM trap inside porous filter wall, where the calculation domain is shown by dotted line

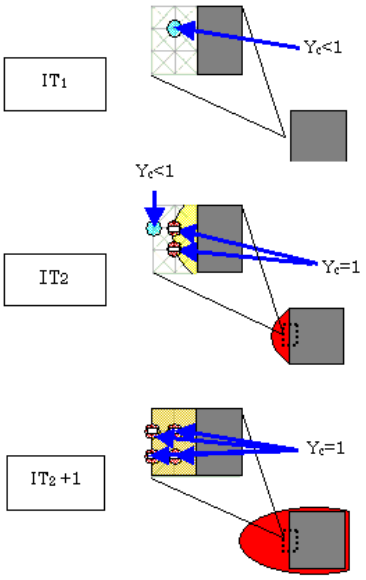

Fig. 2 Soot deposition model

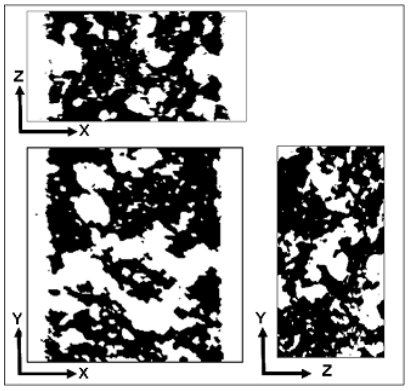

Fig. 3 CT images of the filter at *xy*, *yz*, *xz* planes with area of 400 μm (*x*) × 400 μm (*y*) × 200 μm (*z*), where complex porous structure with variety of pore size is well observed

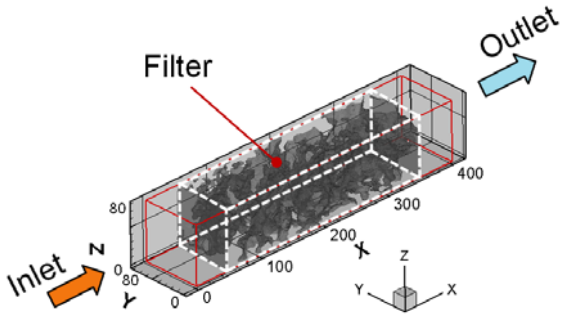

Fig. 4 Calculation domain with the coordinate system

(a)

(b)

(c)

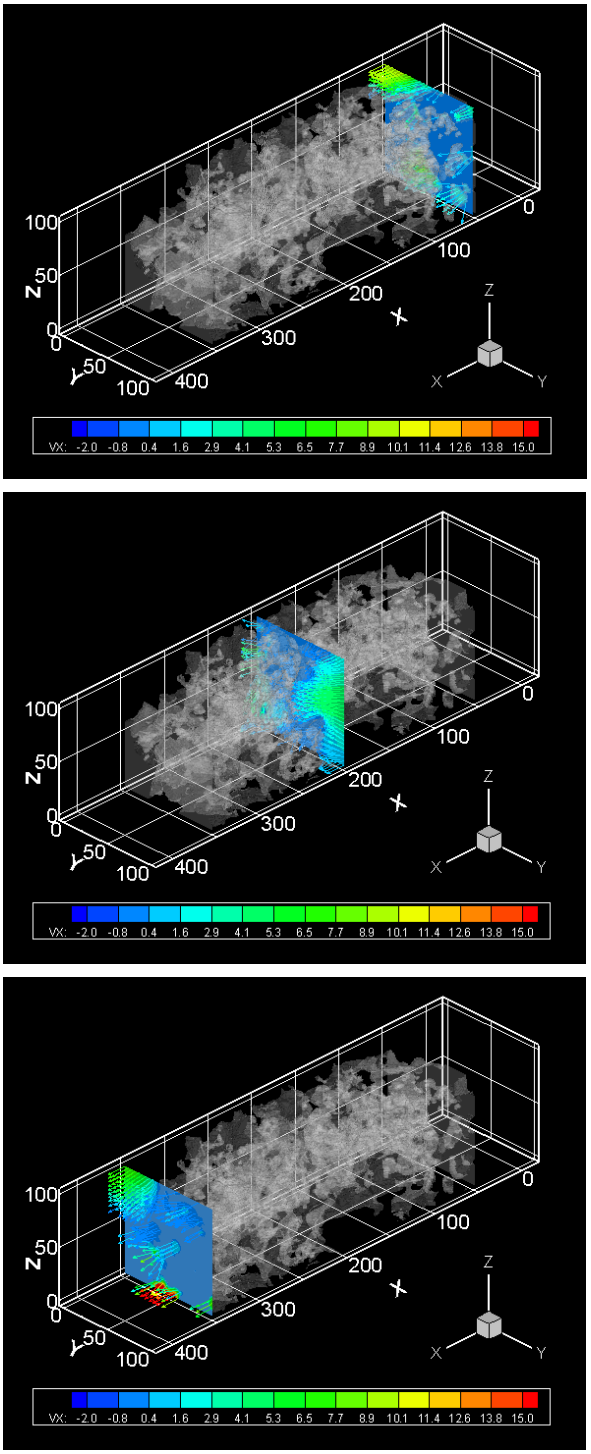

Fig. 5 Flow field inside DPF with filter substrate shown by gray region; (a) x = 50 μm, (b) x = 200 μm, and (c) x = 350 μm. The unit of velocity in flow direction of x is m/s. Inflow velocity is 1 m/s, and flow without soot deposition is considered.

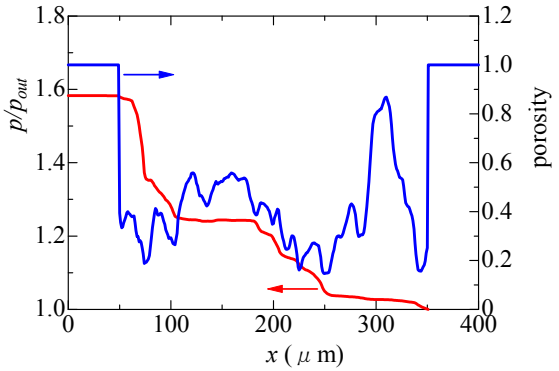

Fig. 6 Distributions of pressure and porosity across the filter wall. Inflow velocity is 1 m/s, and flow without soot deposition is considered.

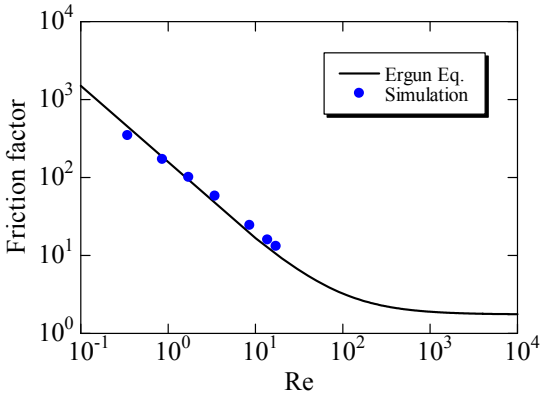

Fig. 7 Variations of friction factor with the Reynolds number, compared with the Ergun equation. Inflow velocity is in the range of 0.2 to 20 m/s. Flow without soot deposition is considered.

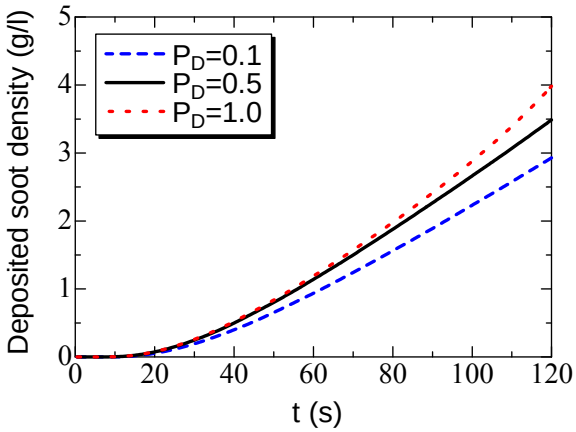

Fig. 8 Deposited soot density in DPF at P_D=0.1, 0.5, and 1.0. Inflow velocity is 1 m/s.

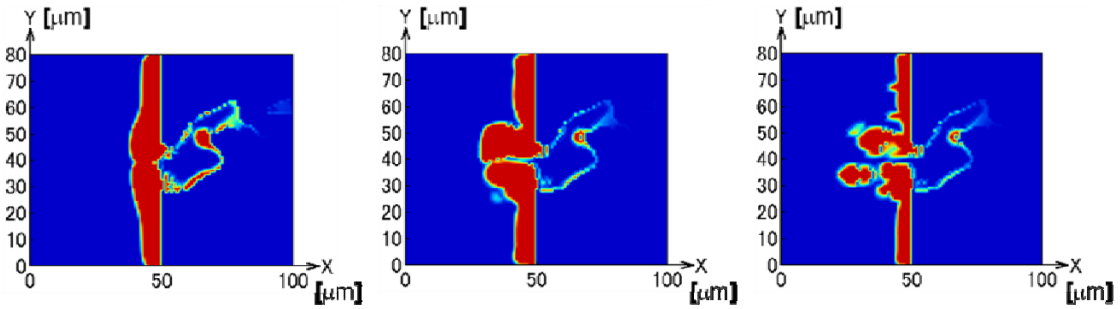

(a) (b) (c)

Fig. 9 Profiles of soot deposition region in *xy* plane at the region of filter wall surface; (a) P_D=0.1, (b) P_D=0.5, (c) P_D=1.0. Inflow velocity is 1 m/s.

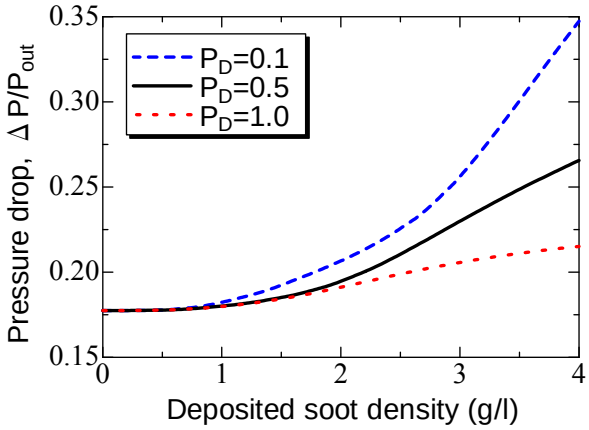

Fig. 10 Relationship between deposited soot density and pressure drop across the filter wall. Inflow velocity is 1 m/s.